# Nanoscale Strontium Titanate Photocatalysts for Overall Water Splitting

**Troy K. Townsend,[†] Nigel D. Browning,[‡] and Frank E. Osterloh[†,*]**

[†]Department of Chemistry, University of California, Davis, One Shields Avenue, Davis, California 95616, United States, and [‡]Chemical Imaging, Chemical and Materials Sciences Division, Pacific Northwest National Laboratory, Richland, Washington, United States

**ABSTRACT**

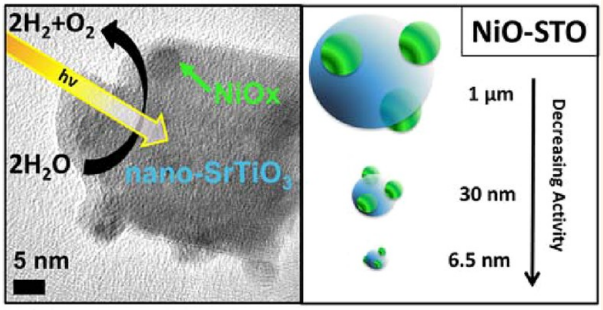


$SrTiO_3$ (STO) is a large band gap (3.2 eV) semiconductor that catalyzes the overall water splitting reaction under UV light irradiation in the presence of a NiO cocatalyst. As we show here, the reactivity persists in nanoscale particles of the material, although the process is less effective at the nanoscale. To reach these conclusions, Bulk STO, 30 ± 5 nm STO, and 6.5 ± 1 nm STO were synthesized by three different methods, their crystal structures verified with XRD and their morphology observed with HRTEM before and after NiO deposition. In connection with NiO, all samples split water into stoichiometric mixtures of $H_2$ and $O_2$, but the activity is decreasing from 28 $\mu$mol $H_2$ $g^{-1}$ $h^{-1}$ (bulk STO), to 19.4 $\mu$mol $H_2$ $g^{-1}$ $h^{-1}$ (30 nm STO), and 3.0 $\mu$mol $H_2$ $g^{-1}$ $h^{-1}$ (6.5 nm STO). The reasons for this decrease are an increase of the water oxidation overpotential for the smaller particles and reduced light absorption due to a quantum size effect. Overall, these findings establish the first nanoscale titanate photocatalyst for overall water splitting.

**KEYWORDS:** photocatalyst · photolysis · complete water splitting · solar fuel · nanoscale

The photocatalytic water splitting reaction is the most promising process to convert photochemical energy from the sun directly into high purity chemical fuel (hydrogen). According to a recent DOE report, suspended heterogeneous photocatalysts operating at 10% solar energy conversion efficiency are theoretically able produce hydrogen fuel at a cost of $1.63/kg $H_2$.[1] This is considerably cheaper than hydrogen produced from photoelectrochemical (PEC) cells or from the combination of photovoltaic (PV) cells with water electrolyzers. Inorganic nanomaterials are particularly interesting as photocatalysts for the water splitting reaction. Because of their small size, full light penetration can be achieved, and even short-lived charge carriers can reach the interface. The positive effects of nanoscaling on photocatalytic activity have been documented for $IrO_2$,[2] $Fe_2O_3$,[3−7] $MnO_2$,[8−10] all of which have been shown to photooxidize water in the presence of an electrical or chemical bias. A disadvantage of nanomaterials is that on this size scale, space charge layers are not effective for separating electron hole pairs, and recombination is enhanced in the absence of a bias. This is one of the reasons that nanoscale catalysts for *overall water splitting* are very rare. So far only three systems have been reported in the literature, all of which require deep ultraviolet light ($\lambda$ < 300 nm) for operation. Kudo's group showed that $LiNbO_3$ nanowires (70 nm × 10 $\mu$m) can split water after modification with $RuO_2$ cocatalyst particles. At 254 nm, the quantum yield was estimated as 0.7%.[11] Yan *et al.* reported overall water splitting with $RuO_2$-modified $Zn_2GeO_4$ nanorods (100 × 150 nm) under UV light from a 400 W Hg UV lamp to excite the large bandgap (>4.5 eV) of the material.[12] In 2011, Domen's group reported overall water splitting with aggregates of NiO-loaded $NaTaO_3$ nanocrystals (20 and 40 nm), but deep ultraviolet light ($\lambda$ < 300 nm) was necessary for catalyst operation.[13] These studies are very encouraging, but significant improvement of the efficiency and an extension of the light absorption range will be required before these systems can ever be useful for true solar energy to fuel conversion. This will require a deeper understanding of the interplay of energetics and the kinetics in such catalysts. Here, we describe such relationships for nano-NiO−$SrTiO_3$ (NiO−STO)—the first nanoscale titanate photocatalyst for overall water splitting. With its 3.2 eV bandgap, STO allows considerably better

* Address correspondence to fosterloh@ucdavis.edu.

Received for review June 15, 2012 and accepted July 22, 2012.

**Published online July 22, 2012**
10.1021/nn302647u

light absorption than the germanates, tantalates, and niobates mentioned above. Another desirable feature of the NiO−STO system is that no rare elements are required for function. Consequently, there is significant interest in this catalyst type.[14−28] We find that 30 nm sized NiO−STO composites can split water with an activity only slightly lower (19.4 $\mu$mol $H_2$ $g^{-1}$ $h^{-1}$) than that of bulk NiO−$SrTiO_3$ (28 $\mu$mol $H_2$ $h^{-1}$ $g^{-1}$). The estimated quantum efficiency is 0.041% at 315 nm (based on 50 mg of the catalyst). When the size of the titanate particles is reduced further, the activity drops significantly, due to the combination of a quantum size effect leading to lower light absorption, and due to slower water oxidation kinetics. These results establish a lower size limit (30 nm diameter) for photocatalysts based on $SrTiO_3$, and suggest that improvements of the activity should target water oxidation kinetics and charge separation in this system.

## RESULTS AND DISCUSSION

Syntheses of the three types of STO (bulk, 30 nm, and 6.5 nm) are summarized in Scheme 1. Bulk STO was prepared from $TiO_2$ and $SrCO_3$ using a high temperature solid-state reaction. As the TEM in Figure 1A shows, the material forms 0.1−1.0 $\mu$m particles with ill-defined surface features and of likely polycrystalline structure.[29] Nanoscale STO particles were synthesized through a hydrothermal synthesis from $TiO_2$, $Sr(OH)_2$, and KOH.[30]

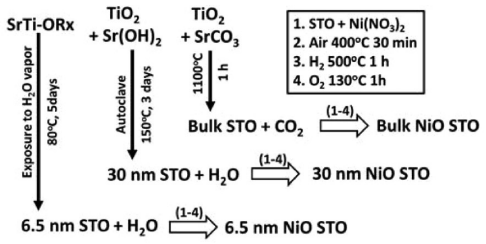


**Scheme 1. Synthesis of Bulk NiO STO, 30 nm NiO STO and 6.5 nm NiO STO with reduction/oxidation pre-treatment to activate the NiO*x* (0 < *x* < 1) cocatalyst.**

According to TEM (Figure 1B), particles are mostly of cubic appearance with edge lengths of 25−60 nm (average value of 30 nm). A third variety of STO was obtained by exposing 10 mL of 0.7 M solution of the bimetallic precursor (SrTi-$(OCH_2CH(CH_3)OCH_3)_6$ in *n*-butanol/3-methoxy-propanol) to 100 mL water vapor under controlled conditions.[31] This produces agglomerated 6.0 ± 1.0 nm STO nanocrystals (Figure 1C), henceforth referred to as 6.5 nm STO.

The crystal structures of the materials were verified with powder X-ray diffraction (Figure 2). All samples are phase pure, based on the diffraction patterns. For 30 nm STO and 6.5 nm STO, crystal domain sizes were estimated from the diffraction peak widths (at half-maximum) using the Scherrer equation. The calculated values of 30 and 6.5 nm agree well with the TEM images of these compounds. To obtain viable catalysts for overall water splitting, NiO was deposited on each type of STO, according to Scheme 1, by impregnating the solids in aqueous $Ni(NO_3)_2$, followed by calcination in air (400 °C), hydrogen (500 °C), and then oxygen atmosphere (130 °C) at the indicated temperatures.

TEM images of bulk NiO STO, 30 nm NiO STO, and 6.5 nm NiO STO are shown in Figure 1D−F. *Z*-contrast imaging for bulk STO verified the presence of $NiO_x$ ($0 \leq x \leq 1$) cocatalyst particles due to the darker contrast. In some cases, Ni(0) particles could also be identified,

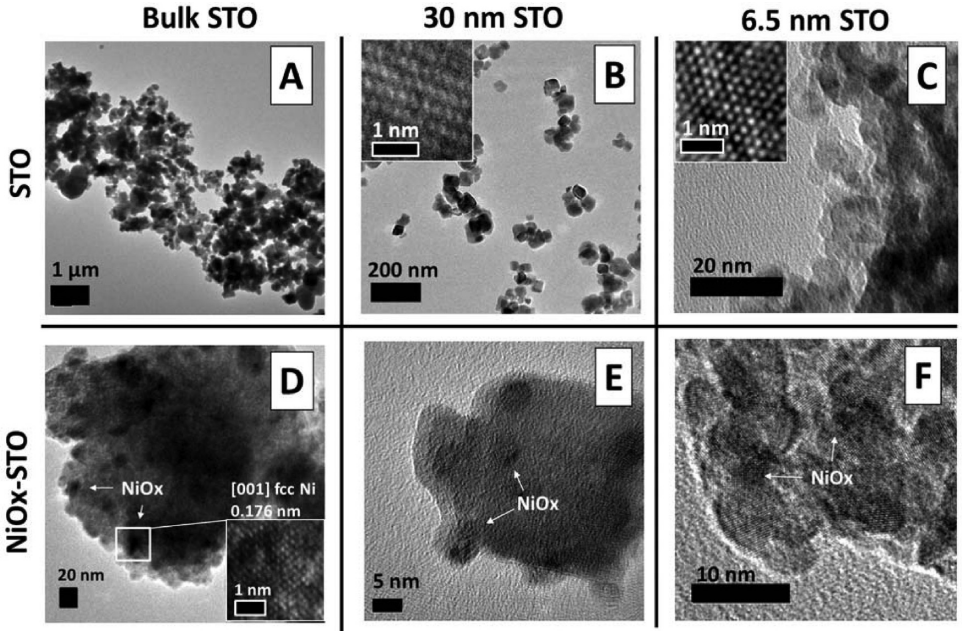


**Figure 1. HRTEMs of Bulk STO (A), 30 nm STO (B), 6.5 nm STO (C), bulk NiO STO with inset of Ni particle (D), 30 nm NiO STO (E), and 6.5 nm NiO STO (F).**

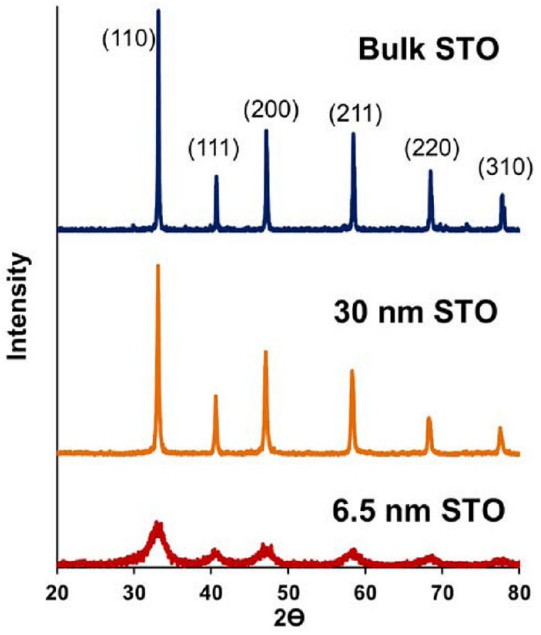


**Figure 2. Powder X-ray diffraction patterns of bulk STO, 30 nm STO, and 6.5 nm STO.**

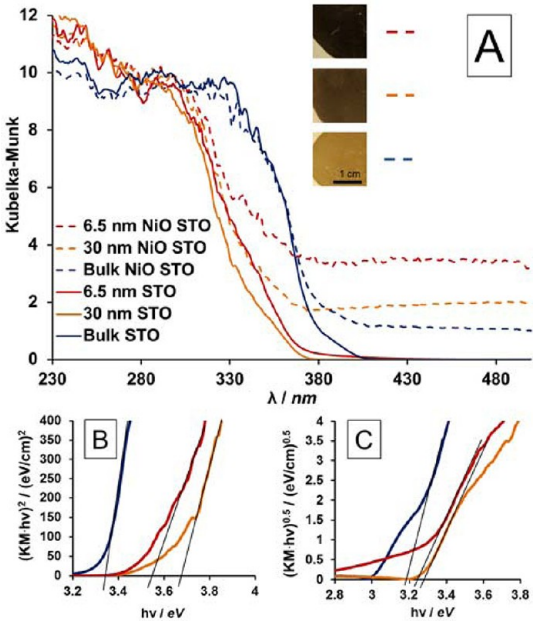


**Figure 3. Kubelka–Munk diffuse reflectance of unmodified STO powders and NiOx attached STO catalysts (A). Tauc plot for allowed direct transitions (B) and allowed indirect transitions (C) of the unmodified STO catalysts.**

based on atomic spacing (Figure 1D). The $NiO_x$ sizes are between 10 and 50 nm (Figure 1D) for bulk STO and 5–10 nm for 30 nm STO (Figure 1E). The decrease in $NiO_x$ particle size is expected from heterogeneous nucleation theory, which predicts an increase in nucleation sites on the larger surface of the smaller STO particles, and consequentially, smaller NiO particles at the end of the growth period. No discrete NiO particles could be observed for the 6.5 nm STO sample (Figure 1F) due to low contrast and agglomeration.

The attachment of $NiO_x$ can also be seen in the optical properties of the materials (Figure 3). $NiO_x$ deposition is accompanied by color change (insert in Figure 3A) due to the broad visible light absorption of nickel and the ultraviolet absorption of NiO (3.2 eV). The smallest 6.5 nm NiO STO appears dark black, 30 nm NiO STO is dark gray, and bulk NiO STO appears light gray (Figure 3 photos). In contrast, the Ni-free materials are white powders with no absorption in the visible. According to the Tauc plots in Figure 3B,C, bulk STO has optical transitions related to a direct bandgap at 3.3 eV and to an indirect bandgap at 3.2 eV. The indirect transition was previously assigned to O 2p and Ti 3d states and the direct transition to O 2p to Sr 4d states.[32] 30 nm STO and 6.5 nm STO also show direct and indirect transitions, but all occur at higher energy (at 3.3–3.7 eV) than for the bulk form. This indicates an incipient quantum size effect in the smaller particles. Such an effect would be expected from the value of the Bohr-exciton radius for $SrTiO_3$ (6.25 nm).[33] In 6.5 nm STO the increase of bandgap is partially obscured by an absorbance tail in the visible region (see Figure 3C). This tail appears to be a result of midgap defect states

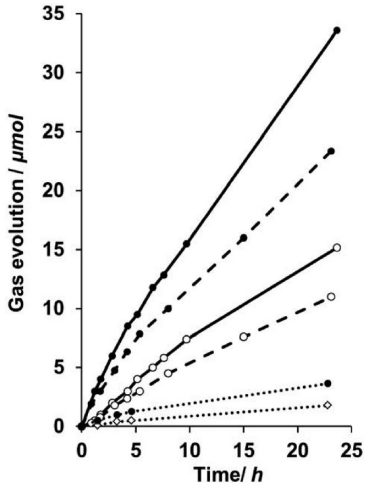


**Figure 4. $H_2$ (●) and $O_2$ (○) evolution from bulk NiO STO (solid line), 30 nm NiO STO (dashed line), and 6.5 nm NiO STO (dotted line) in 50 mL of water at pH = 7 under full spectrum irradiation (~26.3 mW $cm^{-2}$ in the UV from 250 to 380 nm). The catalyst amount was 50 mg (272 μmol based on $SrTiO_3$). Rates were determined for the 5–24 h time period, when $H_2$ evolution was linear.**

that are due to the greater specific surface area (smaller crystal size) of this material. Crystal defects are also due to the low synthesis temperature (80 °C, compared to 150 and 1100 °C for the other materials).

To assess catalytic activity of the three compounds, equal amounts of these catalysts (50 mg) were suspended in pure water and irradiated with a 300 W Xe arc lamp. Stoichiometric $H_2$ and $O_2$ evolution was observed in all cases (Figure 4). Rates slightly decreased after 5 h, but remained stable for the duration

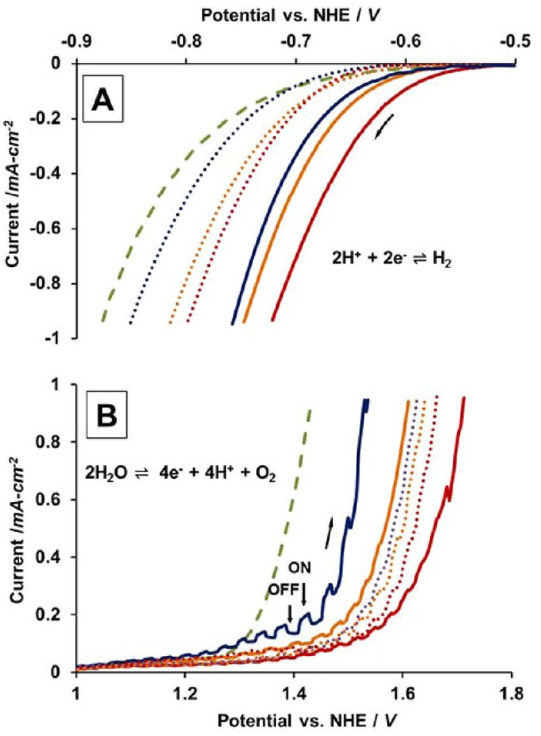


**Figure 5. Electrochemical scans (10 mV $s^{-1}$) on $NiO_x$-STO films on gold in 0.25 M $Na_2HPO_4/NaH_2PO_4$ buffer (pH = 7). All potentials are *vs* NHE. Chopped light during the anodic sans (B) reveals small photocurrents. Dotted blue = bulk STO, solid blue = bulk NiO STO, dotted orange = 30 nm STO, solid orange = 30 nm NiO STO, dotted red = 6.5 nm STO, solid red = 6.5 nm NiO STO, dashed green = plain NiO.**

of the experiments (24 h). Bulk NiO STO had the highest photocatalytic activity (28 $\mu$mol $g^{-1}$ $h^{-1}$), followed by 30 nm NiO STO (19.4 $\mu$mol $g^{-1}$ $h^{-1}$), and 6.5 nm NiO STO (3.0 $\mu$mol $g^{-1}$ $h^{-1}$) (Figure 4). Reference experiments using a lower (1.5 wt %) and a higher (20 wt %) NiO loading on 30 nm NiO−STO resulted in lower water splitting activity (12 and 6.5 $\mu$mol $H_2$ $g^{-1}$ $h^{-1}$, respectively), and no activity for the 6.5 nm NiO STO sample. Therefore, all experiments were conducted with samples containing 3 wt.% NiO.

To determine the reasons for the decreasing activity with decreasing size, the electrochemical overpotentials of the catalysts for water oxidation and water reduction were measured. Potential−current scans of films of the $NiO_x$-free and $NiO_x$-loaded catalysts on gold foil in 0.1 M KCl solution at pH = 7 are shown in Figure 5.

Under these conditions, the proton reduction potentials occur in the following order: Bulk STO (−0.85 V) > 30 nm STO (−0.81 V) > 6.5 nm STO (−0.80 V); that is, the smallest particles reduce protons the easiest. Attachment of $NiO_x$ cocatalysts moves all proton reduction overpotentials to lower values (by 6−9 mV), but the overall order remains the same. Interestingly, water oxidation potentials show an inverted trend: 6.5 nm STO (+1.66 V) > 30 nm STO (+1.64 V) > bulk STO (+1.62 V); that is, here the bulk material oxidizes

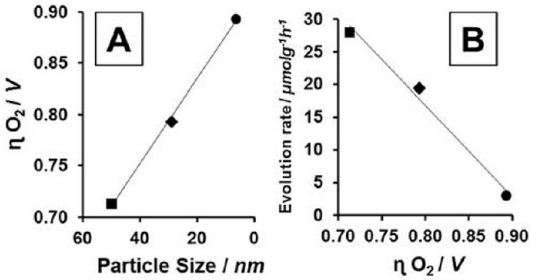


**Figure 6. (A) Water oxidation overpotential *versus* particle size; (B) water oxidation potential *versus* gas evolution rate. Squares, bulk NiO STO; diamonds, 30 nm NiO STO; circles, 6.5 nm NiO STO. Overpotentials are calculated on the basis of the theoretical water oxidation potential of +0.817 V (NHE), at pH 7.**

water the easiest. Again, $NiO_x$ attachment does reduce the overpotentials slightly, but does not change the relative reactivity order. This suggests that NiO*x* may be directly involved in the water oxidation reaction. This question is currently under investigation in the laboratory.

At present, the reason for the variation of redox potentials with $SrTiO_3$ particle size is unclear. One possible explanation is a increase of the $SrTiO_3$ surface acidity with decreasing particle size, as has been recently reported for nanoscale $TiO_2$ particles.[34] Higher surface acidity would translate into higher proton coverage (at fixed solution pH), and lower proton reduction potential (higher water oxidation potential). This would explain the trend observed above.

Figure 6 shows plots of the particle size against water oxidation overpotentials $\eta_{ox}$ and against photocatalytic $H_2/O_2$ evolution rates *R*. The correlation between $\eta_{ox}$ and *R* is evident. This proves that water oxidation kinetics are limiting the catalyst performance under illumination. This result is somewhat surprising because photochemical and electrochemical water oxidation proceed by different mechanisms. The former is driven by the photoholes in the valence band, whereas the latter is driven by empty states in the conduction band. The correlation between $\eta_{ox}$ and *R* suggests that both routes proceed *via* similar reaction intermediates (*e.g.*, hydroxyl radicals), and that the energetics of those intermediates are limiting the water oxidation rate. Indeed the trend observed here is not unique. We have previously reported that the photocatalytic $H_2$ and $O_2$ evolution rates in nanomaterials can be correlated with the respective electrochemical overpotentials.[35−37]

The photoenergetics of the three $SrTiO_3$ materials were also investigated, employing photoelectrochemical scans on films in aqueous 0.1 M KCl solution that contained 10% (vol) methanol. Corresponding data is shown in Figure 7 and listed in Table 1. For bulk STO, photocurrents were found to be small (10 $\mu$A $cm^{-2}$), but exhibited a clear onset potential $E_{ph}$ at −0.87 V vs NHE. For n-type semiconductors, including $SrTiO_3$, the

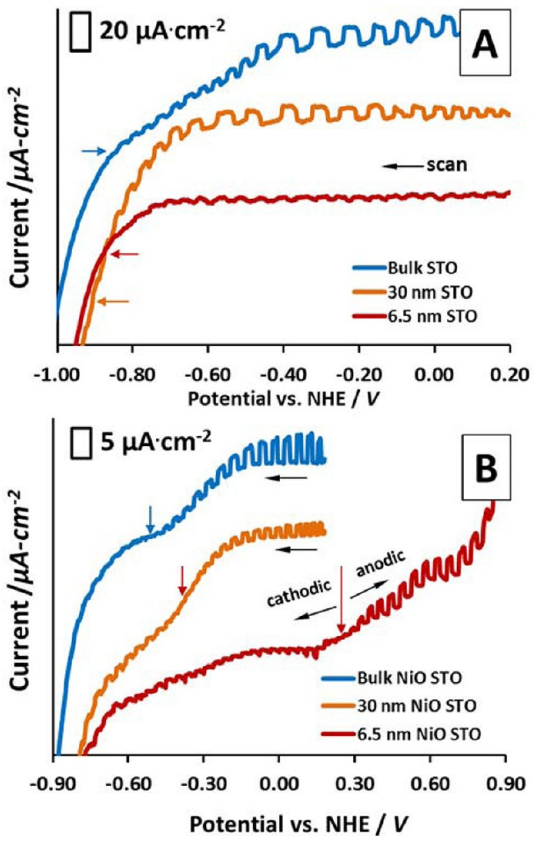


**Figure 7. Photocurrent scans of bulk STO, 30 nm STO, 6.5 nm STO (A), and bulk NiO STO, 30 nm NiO STO, 6.5 nm NiO STO (B) films on Au substrate, 10 mV $s^{-1}$, at pH = 7 in 0.1 M KCl/10% vol. methanol. Arrows indicate photo-onset potentials $E_{ph}$. In all samples, a reversal of the photocurrent direction occurs at $E_{applied} < E_{ph}$.**

**TABLE 1. Electrochemical Water Reduction/Oxidation Potentials and Photo-onset Potential $E_{ph}$ (V *vs.* NHE at 0.90 mA $cm^{-2}$) with Band Gap Energy, $E_G$ (eV)**

| catalyst | proton reduction potential (V) | water oxidation potential (V) | $E_{ph}$ (V) | $E_G$ (eV) |
|---|---|---|---|---|
| bulk STO | −0.85 | +1.62 | −0.87 | 3.32 |
| 30 nm STO | −0.81 | +1.64 | −0.94 | 3.67 |
| 6.5 nm STO | −0.80 | +1.66 | −0.90 | 3.55 |
| bulk NiO STO | −0.76 | +1.53 | −0.49 | 3.32 |
| 30 nm NiO STO | −0.75 | +1.61 | −0.36 | 3.67 |
| 6.5 nm NiO STO | −0.72 | +1.71 | +0.27 | 3.55 |

photo-onset potential $E_{ph}$ serves as an approximation of the conduction band edge. Indeed the experimental value compares well with the literature for the conduction band edge of $SrTiO_3$.[38] For 30 nm STO the onset potential value was shifted in the negative direction (−0.94 V). A shift of $E_{CB}$ to more reducing potentials can be taken as the second manifestation of the quantum size effect, in addition to the blue-shifted absorption in the optical spectra. For 6.5 nm STO, a $E_{ph}$ value similar to that of bulk STO is found (−0.90 V). However, the photocurrent for this material is very weak, possibly obscuring a more negative value, closer to that of 30 nm STO.

When $NiO_x$ cocatalysts are fused onto the STO particles, photocurrents get smaller (<5 $\mu Acm^{-2}$) and photo-onsets shift to more positive values for all catalysts (Figure 7). For bulk NiO STO, $E_{ph}$ is at −0.49 V, and for 30 and 6.5 nm, NiO−STO values are found at −0.36 and +0.27 V, respectively. These very positive shifts are due to Fermi level equilibration between STO and NiO. Significant, but smaller (60−240 mV) positive shifts of the photo-onset potentials were previously found in nanoscale niobates and titanates after the binding of Pt and $IrO_x$ nanoparticles.[35,39] Nickel oxide is a p-type semiconductor with a 3.31 eV band gap and a flatband potential of +0.67 V (NHE).[40] The experimental $E_{ph}$ values for bulk NiO STO fall between those observed for NiO and STO alone. Due to the p-type character of NiO, the new $E_{ph}$ values can no longer be taken as the conduction band edge position of STO, but must be interpreted as the common Fermi level of the NiO−STO system. Another feature of the electrochemical scans is an inversion from anodic to cathodic photocurrents that occurs negative of the $E_{ph}$ potentials. This inversion is found for all samples, but it is most pronounced for the 6.5 and 30 nm STO particles. In small particles, the space charge layer is not effective for separating charge,[41−43] and so the sign of the photocurrent is due to other factors. In the present case, we hypothesize that the direction of photocurrent is determined by the polarity of the electrical double layer at the semiconductor electrode. Further studies on the photocurrent inversion effect are underway.

## CONCLUSION

We have described overall photocatalytic water splitting with bulk and two types of nanoscale NiO*x*−$SrTiO_3$ particles. All materials perform under UV light, but the 30 nm particles are about 35% less active than the bulk, and 6.5 nm have only 10% of the activity. The decrease of activity is attributed to a combination of factors; the most important ones are reduced light absorption due to the beginning of a quantum size effect in the 30 and 6.5 nm samples, and an observed increase in water oxidation potentials with the smaller particles. Thus, for full activity under UV light, catalyst particles should be larger than 30 nm. Also, the significant overpotentials for water reduction and oxidation suggest that optimization of activity with $SrTiO_3$ could be achieved by adding more effective cocatalysts. The positive effect of the $NiO_x$ coating on both water reduction and oxidation potentials implies that $NiO_x$ is directly involved in both reactions. Additional studies on the detailed mechanism of water splitting with NiO−$SrTiO_3$ are underway in this laboratory. Lastly, we note that 30 nm NiO $SrTiO_3$ is only the

fourth nanoscale catalyst for overall water splitting, apart from $RuO_2$−$LiNbO_3$ nanowires (70 nm × x 10 $\mu$m),[11] $RuO_2$−$Zn_2GeO_4$ nanorods (100 × 150 nm),[12] and NiO−$NaTaO_3$ nanocrystals (20 and 40 nm).[13] Owing to its smaller bandgap of 3.2 eV, nano NiO−STO is active under near UV conditions, whereas the other nanoscale catalysts require deep UV light (<300 nm) for operation.

## METHODS

**Chemicals.** KOH 99.9%, $Sr(NO_3)_2$ 99.9%, Degussa P25 $TiO_2$, $NH_4OH$ 99.9%, $Ni(NO_3)_2 \cdot (H_2O)_6$ 99.9%, and ammonium hydroxide were purchased from Fisher Scientific, Pittsburgh, PA. Strontium titanium bimetallic alkoxide (SrTi-$(OCH_2CH(CH_3)OCH_3)_6$; 0.7 M in *n*-butanol/3-methoxypropanol; Gelest, Inc.) was used as received. $Sr(OH)_2$ was prepared by precipitation at room temperature from $Sr(NO_3)_2$ and KOH in water. They were of reagent quality and were used as received. Water was purified to 18 MΩcm resistivity using a *Nanopure* system.

**Particle Synthesis.** Bulk-$SrTiO_3$ particles were synthesized *via* a high temperature solid state process[29] where 0.021 mol, 1.74 g of P25 $TiO_2$ was mixed and sonicated for 10 min with 0.026 mol, 5.53 g $Sr(NO_3)_2$ in a 1:1.2 molar ratio in 200 mL of water to produce precursors for 4 g of $SrTiO_3$. 54 mL of aqueous oxalic acid (0.4 M, 1:1 molar ratio with Sr) was added dropwise to the solution under vigorous stirring. Concentrated ammonium hydroxide was added slowly to increase the pH of the solution to 6.5 in order to precipitate strontium oxalate crystals onto the 25 nm $TiO_2$ particle surfaces *via* heterogeneous nucleation.[44] When precipitation was complete, the white solid was centrifuged and washed eight times in 50 mL of water, followed by drying in air at 100 °C. This precursor was calcined in a Thermolyne 79300 Tube Furnace to 1100 °C for 1 h with a heating rate of 10 °C $min^{-1}$. After being cooled to room temperature, the white solid was washed twice in 50 mL of 5 M $HNO_3$ to remove excess $SrCO_3$ followed by repeated water washes until the supernatant reached a pH of 7. Phase purity was confirmed by powder X-ray diffraction.

Nano-$SrTiO_3$ particles (30 nm) were synthesized *via* a hydrothermal autoclave route.[30] $TiO_2$ (0.18 g, 2.3 mmol) was mixed in a 20 mL aqueous solution of 1.26 g, 23 mmol of KOH and 0.508 g, 2.3 mmol of $Sr(OH)_2$ in a 30 mL Teflon container sealed in a pressure vessel. This mixture was heated to 150 °C for 3 days. The vessel was cooled to room temperature, and the formed white powder was washed with water until the supernatant reached a pH of 7 and then dried at 100 °C in air.

Nano-$SrTiO_3$ particles (6.5 nm) were synthesized following a vapor diffusion sol−gel technique[31] where 10 mL of a 0.7 M solution of SrTi-$(OCH_2CH(CH_3)OCH_3)_6$ in *n*-butanol/3-methoxypropanol (Gelest, Inc.) was heated under $N_2$ atmosphere at 80 °C, exposed to water vapor from an adjacent flask of water (at 25 °C) for 72 h. The resulting off-white gel was washed in ethanol and dried at 100 °C to yield 6.5 nm STO.

**NiO Loading.** The $SrTiO_3$ particles (200 mg, 1.10 mmol) were added to 20 mL of an aqueous $Ni(NO_3)_2 \cdot 6H_2O$ solution (0.023 g, 3 wt % loading of NiO:STO) and thoroughly mixed in a sonication bath for 10 min. This solution was dried at 100 °C and then calcined for 30 min at 400 °C in air. The air above the solid was flushed with $N_2$ and then replaced by $H_2$, and the sample was heated to 500 °C for 1.5 h to reduce nickel. The final product was obtained after another 30 min of heating at 130 °C in an $O_2$ atmosphere as described in the literature.[45]

High-resolution transmission electron microscopy (HRTEM) images were taken using a JEOL 2500SE 200 kV TEM. To prepare samples, copper grids with a carbon film were dropped into aqueous dispersions of the samples followed by washing with water and air drying. UV−vis diffuse reflectance spectra were recorded on dried powders on white Teflon tape using a Thermo Scientific Evolution 220 spectrometer. The reflectance data were converted to the Kubelka−Munk function as $f(R) = (1 - R)^2(2R)^{-1}$ *versus* wavelength to correct for scattering, which is plotted in Figure 3. For electrochemical measurements, thin films of the catalysts were prepared on a gold foil electrode (1.0 $cm^2$) by drop coating and drying at 25 °C. A wire was attached to the bare gold back with conductive carbon tape and sealed with adhesive. The electrode was placed into a $N_2$-purged 3-electrode cell with a Pt counter electrode and a saturated calomel reference electrode connected to the cell with a KCl salt bridge. The cell was filled to 50 mL with 0.25 M $Na_2HPO_4/NaH_2PO_4$ buffer solution at pH 7 and purged with $N_2$ to remove oxygen. Cyclic voltammetry scans were taken at 50 mV/s. The system was calibrated using the redox potential of $K_4(Fe(CN)_6)$ at +0.358 V (NHE). Photolectrochemcial scans were conducted in 0.1 M KCl with 10% (vol) added methanol. The rate of photochemical hydrogen and oxygen evolution from each catalyst was determined by irradiating 50 mg of NiO−STO dispersed in 50 mL of water. Irradiations were performed in a quartz round-bottom flask with a 300 W Xe arc lamp (26.3 mW $cm^{-2}$ at the flask $\lambda$ = 250−380 nm), measured with a GaN photodetector. The airtight irradiation system connects a vacuum pump and a gas chromatograph (Varian 3800) with the sample flask to quantify the amount of gas evolved, using area counts of the peaks and the identity of the gas from the calibrated carrier times. Prior to irradiation, the flask was evacuated down to 5 Torr and purged with argon gas. This cycle was repeated until the chromatogram of the atmosphere above the solution indicated that the sample did not contain hydrogen, oxygen, or nitrogen.

Powder XRD scans were conducted with a Scintag XRD, at a wavelength of $\lambda$ = 0.154 nm with 2 mm tube slit divergence, 4 mm scatter, 0.5 mm column scatter, and 0.2 mm receiving widths. The full width at half-maximum (fwhm) values of the peaks were calculated with Thermo ARLDMSNT software (version 1.39-1).

*Conflict of Interest:* The authors declare no competing financial interest.

*Acknowledgment.* Financial support was provided by Research Corporation for Science Advancement (Scialog award), by the National Science Foundation (NSF, Grants 0829142 and 1133099) and by the U.S. Department of Energy under Grant FG02-03ER46057. T.K.T. thanks NSF for a graduate student fellowship.

## REFERENCES AND NOTES

1. Baum, G. N.; Perez, J.; Baum, K. N. *Technoeconomic Analysis of Photoelectrochemical (PEC) Hydrogen Production*; Directed Technologies: Arlington, VA, **2009**; pp 1−127.
2. Frame, F. A.; Townsend, T. K.; Chamousis, R. L.; Sabio, E. M.; Dittrich, T.; Browning, N. D.; Osterloh, F. E. Photocatalytic Water Oxidation with Non-sensitized $IrO_2$ Nanocrystals under Visible and UV Light. *J. Am. Chem. Soc.* **2011**, *133*, 7264–7267.
3. Townsend, T. K.; Sabio, E. M.; Browning, N. D.; Osterloh, F. E. Photocatalytic Water Oxidation with Suspended Alpha-$Fe_2O_3$ Particles—Effects of Nanoscaling. *Energy Environ. Sci.* **2011**, *4*, 4270–4275.
4. Khan, S. U. M.; Akikusa, J. Photoelectrochemical Splitting of Water at Nanocrystalline *n*-$Fe_2O_3$ Thin-Film Electrodes. *J. Phys. Chem. B* **1999**, *103*, 7184–7189.
5. Beermann, N.; Vayssieres, L.; Lindquist, S. E.; Hagfeldt, A. Photoelectrochemical Studies of Oriented Nanorod Thin Films of Hematite. *J. Electrochem. Soc.* **2000**, *147*, 2456–2461.
6. Duret, A.; Gratzel, M. Visible Light-Induced Water Oxidation on Mesoscopic Alpha-$Fe_2O_3$ Films Made By Ultrasonic Spray Pyrolysis. *J. Phys. Chem. B* **2005**, *109*, 17184–17191.

7. Cesar, I.; Kay, A.; Martinez, J. A. G.; Gratzel, M. Translucent Thin Film $Fe_2O_3$ Photoanodes for Efficient Water Splitting by Sunlight: Nanostructure-Directing Effect of Si-Doping. *J. Am. Chem. Soc.* **2006**, *128*, 4582–4583.
8. Hocking, R. K.; Brimblecombe, R.; Chang, L. Y.; Singh, A.; Cheah, M. H.; Glover, C.; Casey, W. H.; Spiccia, L. Water-Oxidation Catalysis by Manganese in a Geochemical-like Cycle. *Nat. Chem.* **2011**, *3*, 461–466.
9. Sakai, N.; Ebina, Y.; Takada, K.; Sasaki, T. Photocurrent Generation from Semiconducting Manganese Oxide Nanosheets in Response to Visible Light. *J. Phys. Chem. B* **2005**, *109*, 9651–9655.
10. Pinaud, B. A.; Chen, Z. B.; Abram, D. N.; Jaramillo, T. F. Thin Films of Sodium Birnessite-Type $MnO_2$: Optical Properties, Electronic Band Structure, and Solar Photoelectrochemistry. *J. Phys. Chem. C* **2011**, *115*, 11830–11838.
11. Saito, K.; Koga, K.; Kudo, A. Lithium Niobate Nanowires for Photocatalytic Water Splitting. *Dalton Trans.* **2011**, *40*, 3909–3913.
12. Yan, S. C.; Wan, L. J.; Li, Z. S.; Zou, Z. G. Facile Temperature-Controlled Synthesis of Hexagonal $Zn_2GeO_4$ Nanorods with Different Aspect Ratios Toward Improved Photocatalytic Activity for Overall Water Splitting and Photoreduction of $CO_2$. *Chem. Commun.* **2011**, *47*, 5632–5634.
13. Yokoi, T.; Sakuma, J.; Maeda, K.; Domen, K.; Tatsumi, T.; Kondo, J. N. Preparation of a Colloidal Array of $NaTaO_3$ Nanoparticles *via* a Confined Space Synthesis Route and Its Photocatalytic Application. *Phys. Chem. Chem. Phys.* **2011**, *13*, 2563–2570.
14. Wrighton, M. S.; Ellis, A. B.; Wolczanski, P. T.; Morse, D. L.; Abrahamson, H. B.; Ginley, D. S. Strontium-Titanate Photoelectrodes—Efficient Photoassisted Electrolysis of Water at Zero Applied Potential. *J. Am. Chem. Soc.* **1976**, *98*, 2774–2779.
15. Domen, K.; Naito, S.; Soma, M.; Onishi, T.; Tamaru, K. Photocatalytic Decomposition of Water-Vapor on an $NiO-SrTiO_3$ Catalyst. *J. Chem. Soc., Chem. Commun.* **1980**, *12*, 543–544.
16. Wagner, F. T.; Somorjai, G. A. Photocatalytic Hydrogen-Production from Water on Pt-free $SrTiO_3$ in Alkali Hydroxide Solutions. *Nature* **1980**, *285*, 559–560.
17. Kumar, A.; Santangelo, P. G.; Lewis, N. S. Electrolysis of Water at $SrTiO_3$ Photoelectrodes—Distinguishing Between the Statistical and Stochastic Formalisms for Electron-Transfer Processes in Fuel-Forming Photoelectrochemical Systems. *J. Phys. Chem.* **1992**, *96*, 834–842.
18. Sayama, K.; Arakawa, H. Effect of $Na_2CO_3$ Addition on Photocatalytic Decomposition of Liquid Water over Various Semiconductor Catalysts. *J. Photochem. Photobiol. A* **1994**, *77*, 243–247.
19. Sayama, K.; Mukasa, K.; Abe, R.; Abe, Y.; Arakawa, H. Stoichiometric Water Splitting into $H_2$ and $O_2$ Using a Mixture of Two Different Photocatalysts and an $IO_3^-/I^-$ Shuttle Redox Mediator Under Visible Light Irradiation. *Chem. Commun.* **2001**, *23*, 2416–2417.
20. Konta, R.; Ishii, T.; Kato, H.; Kudo, A. Photocatalytic Activities of Noble Metal Ion Doped $SrTiO_3$ under Visible Light Irradiation. *J. Phys. Chem. B* **2004**, *108*, 8992–8995.
21. Liu, J. W.; Chen, G.; Li, Z. H.; Zhang, Z. G. Electronic Structure and Visible Light Photocatalysis Water Splitting Property of Chromium-Doped $SrTiO_3$. *J. Solid State Chem.* **2006**, *179*, 3704–3708.
22. Sasaki, Y.; Nemoto, H.; Saito, K.; Kudo, A. Solar Water Splitting Using Powdered Photocatalysts Driven by Z-Schematic Interparticle Electron Transfer without an Electron Mediator. *J. Phys. Chem. C* **2009**, *113*, 17536–17542.
23. Iwashina, K.; Kudo, A. Rh-Doped $SrTiO_3$ Photocatalyst Electrode Showing Cathodic Photocurrent for Water Splitting under Visible-Light Irradiation. *J. Am. Chem. Soc.* **2011**, *133*, 13272–13275.
24. Lehn, J. M.; Sauvage, J. P.; Ziessel, R. Photochemical Water Splitting Continuous Generation of Hydrogen and Oxygen by Irradiation of Aqueous Suspensions of Metal-Loaded Strontium-Titanate. *New J. Chem.* **1980**, *4*, 623–627.
25. Lehn, J. M.; Sauvage, J. P.; Ziessel, R.; Hilaire, L. Water Photolysis by UV Irradiation of Rhodium Loaded Strontium-Titanate Catalysts—Relation between Catalytic Activity and Nature of the Deposit from Combined Photolysis and Esca Studies. *Israel J. Chem.* **1982**, *22*, 168–172.
26. Kudo, A.; Miseki, Y. Heterogeneous Photocatalyst Materials for Water Splitting. *Chem. Soc. Rev.* **2009**, *38*, 253–278.
27. Domen, K.; Naito, S.; Onishi, T.; Tamaru, K. Photocatalytic Decomposition of Liquid Water on a NiO $SrTiO_3$ Catalyst. *Chem. Phys. Lett.* **1982**, *92*, 433–434.
28. Ouyang, S. X.; Tong, H.; Umezawa, N.; Cao, J. Y.; Li, P.; Bi, Y. P.; Zhang, Y. J.; Ye, J. H. Surface-Alkalinization-Induced Enhancement of Photocatalytic $H_2$ Evolution Over $SrTiO_3$-Based Photocatalysts. *J. Am. Chem. Soc.* **2012**, *134*, 1974–1977.
29. Roy, P. K.; Bera, J. Formation of $SrTiO_3$ from Sr-Oxalate and $TiO_2$. *Mater. Res. Bull.* **2005**, *40*, 599–604.
30. Tsumura, T.; Matsuoka, K.; Toyoda, M. Formation and Annealing of $BaTiO_3$ and $SrTiO_3$ Nanoparticles in KOH Solution. *J. Mater. Sci. Technol.* **2010**, *26*, 33–38.
31. Beier, C. W.; Cuevas, M. A.; Brutchey, R. L. Low-Temperature Synthesis of Solid-Solution $Ba_xSr_{1-x}TiO_3$ Nanocrystals. *J. Mater. Chem.* **2010**, *20*, 5074–5079.
32. Benthem, K. v.; Elsasser, C.; French, R. H. Bulk Electronic Structure of $SrTiO_3$: Experiment and Theory. *J. Appl. Phys.* **2001**, *90*, 6156–6164.
33. Mune, Y.; Ohta, H.; Koumoto, K.; Mizoguchi, T.; Ikuhara, Y. Enhanced Seebeck Coefficient of Quantum-Confined Electrons in $SrTiO_3/SrTi_{0.8}Nb_{0.2}O_3$ Superlattices. *Appl. Phys. Lett.* **2007**, *91*, 192105−1–192105−3.
34. Suttiponparnit, K.; Jiang, J.; Sahu, M.; Suvachittanont, S.; Charinpanitkul, T.; Biswas, P. Role of Surface Area, Primary Particle Size, and Crystal Phase on Titanium Dioxide Nanoparticle Dispersion Properties. *Nanoscale Res. Lett.* **2011**, *6*, 1–8.
35. Townsend, T. K.; Sabio, E. M.; Browning, N. D.; Osterloh, F. E. Improved Niobate Nanoscroll Photocatalysts for Partial Water Splitting. *Chemsuschem* **2011**, *4*, 185–190.
36. Townsend, T. K.; Sabio, E. M.; Browning, N. D.; Osterloh, F. E. Photocatalytic Water Oxidation with Suspended Alpha-$Fe_2O_3$ Particles-Effects of Nanoscaling. *Energy Environ. Sci.* **2011**, *4*, 4270–4275.
37. Sabio, E. M.; Chamousis, R. L.; Browning, N. D.; Osterloh, F. E. Photocatalytic Water Splitting with Suspended Calcium Niobium Oxides: Why Nanoscale Is Better Than Bulk—A Kinetic Analysis. *J. Phys. Chem. C* **2012**, *116*, 3161–3170.
38. Nozik, A. J. Photoelectrochemistry: Applications to Solar Energy Conversion. *Annu. Rev. Phys. Chem.* **1978**, *29*, 189–222.
39. Allen, M. R.; Thibert, A.; Sabio, E. M.; Browning, N. D.; Larsen, D. S.; Osterloh, F. E. Evolution of Physical and Photocatalytic Properties in the Layered Titanates $A_2Ti_4O_9$ (A = K, H) and in Nanosheets Derived by Chemical Exfoliation. *Chem. Mater.* **2010**, *22*, 1220–1228.
40. Nakaoka, K.; Ueyama, J.; Ogura, K. Semiconductor and Electrochromic Properties of Electrochemically Deposited Nickel Oxide Films. *J. Electroanal. Chem.* **2004**, *571*, 93–99.
41. Hodes, G.; Howell, I. D. J.; Peter, L. M. Nanocrystalline Photoelectrochemical Cells—A New Concept In Photovoltaic Cells. *J. Electrochem. Soc.* **1992**, *139*, 3136–3140.
42. Hodes, G. Size-Quantized Nanocrystalline Semiconductor-Films. *Israel J. Chem.* **1993**, *33*, 95–106.
43. Liu, D.; Kamat, P. V. Photoelectrochemical Behavior of Thin CdSe and Coupled $TiO_2$ CdSe Semiconductor-Films. *J. Phys. Chem.* **1993**, *97*, 10769–10773.
44. Bera, J.; Sarkar, D. Formation of $BaTiO_3$ from Barium Oxalate and $TiO_2$. *J. Electroceram.* **2003**, *11*, 131–137.
45. Domen, K.; Kudo, A.; Onishi, T. Mechanism of Photocatalytic Decomposition of Water into $H_2$ and $O_2$ over $NiO-SrTiO_3$. *J. Catal.* **1986**, *102*, 92–98.